Chinese Chemical Letters 36 (2025) 110366

Contents lists available at ScienceDirect

Chinese Chemical Letters

journal homepage: www.elsevier.com/locate/cclet

Parallel on-tissue chemical derivatization for enhanced molecular annotation of spatial carbonyl submetabolome

Shuai Guo[a,b,1], Kening Li[a,c,1], Bin Li[a,c,*]

[a] State Key Laboratory of Natural Medicines, China Pharmaceutical University, Nanjing 210009, China
[b] School of Basic Medicine and Clinical Pharmacy, China Pharmaceutical University, Nanjing 210009, China
[c] School of Traditional Chinese Pharmacy, China Pharmaceutical University, Nanjing 210009, China

ARTICLE INFO

Article history:
Received 9 April 2024
Revised 23 July 2024
Accepted 23 August 2024
Available online 7 September 2024

Keywords:
Mass spectrometry imaging
On-tissue chemical derivatization
Parallel derivatization
Carbonyl metabolites
Mass-shift filtering
Spatial distribution similarity

ABSTRACT

Matrix-assisted laser desorption/ionization (MALDI) mass spectrometry imaging (MSI) is an attractive technology for the visualization of metabolite distributions in tissues. However, detection and identification of low-abundance or poorly ionized metabolites remains challenging. Although on-tissue chemical derivatization (OTCD) holds great promise for improving MALDI MS detection sensitivity and selectivity by modification of specific chemical groups, the available methods for subsequent metabolite annotation are limited. Herein, a laser-assisted chemical transfer (LACT)-based parallel OTCD strategy was established for visualizing and annotating carbonyl metabolites in murine brain tissues. Girard's T and Girard's P reagents were applied for parallel OTCD to generate the characteristic *m/z* pairs with a 19.969 Da mass shift (±0.020 Da tolerance) for rapid recognition of derivatized metabolites. The similarity of spatial distribution patterns of each *m/z* pair was further statistically evaluated to remove the ambiguous annotations due to the occurrence of interference compounds. As a result, 90 ion pairs were annotated as candidate carbonyl metabolites, 66 were previously known and 24 were potential unreported carbonyls. Furthermore, the spatial alterations of carbonyl metabolites in the ischemic rat brain were successfully visualized and characterized, including small molecule aldehydes and ketones, long-chain fatty aldehydes, and monosaccharides. This further emphasizes great potential of parallel OTCD strategy for efficient and confident molecular annotation of spatial submetabolomics data associated with brain diseases.

Spatial metabolomics based on mass spectrometry imaging (MSI) has become an imperative tool to spatially delineate and assess the physiological and pathophysiological changes in tissues. It has been widely applied across various research areas such as disease biomarker discovery, therapeutic drug monitoring, natural product dereplication, and pathological mechanism explanation [1-4]. However, owing to the inherent suppression effects and high molecular complexity of tissue samples, relatively low molecular coverage is still an obstacle for current MALDI MSI to characterize the spatial metabolome of biological systems [5]. To overcome this drawback, numerous emerging sample preparation strategies and instrumental advancements, such as novel matrices and corresponding deposition techniques [6], tissue pretreatment methods [7-9], as well as atmospheric pressure matrix-assisted laser desorption/ionization (AP MALDI) and laser post-ionization (*e.g.*, MALDI-2) [10,11], have been proposed to combine with high-resolution mass spectrometry for obtaining a broader molecular coverage. Nevertheless, for certain compounds with low abundance and/or difficult-to-ionize, such as carbonyl metabolites, most of these existing MSI techniques still suffer from limited sensitivity and selectivity, especially when complex biological environments are involved [12].

Currently, on-tissue chemical derivatization (OTCD) has become a valuable strategy to enhance the detection sensitivity of MSI by introducing a rationally designed tagging reagent to react with the common functional group of a submetabolome [13-15]. Further developments in OTCD strategies, such as gel-assisted OTCD [16], vacuum-promoted OTCD [17], and electric field-assisted OTCD [18], have been demonstrated to achieve broader molecular coverage for MALDI MSI. However, the increase in signal intensity *via* general OTCD is still limited, particularly for some carbonyl metabolites (*e.g.*, pyruvic acid, levulinic acid, and dodecanal), which may not be directly detected in tissue sections by MALDI MSI. We have recently developed a laser-assisted chemical transfer (LACT)-based OTCD method, which employs backside laser irradiation of tissue to locally accelerate the derivatization reaction and force

* Corresponding author.
E-mail address: binli@cpu.edu.cn (B. Li).
[1] These authors contributed equally to this work.

https://doi.org/10.1016/j.cclet.2024.110366
1001-8417/

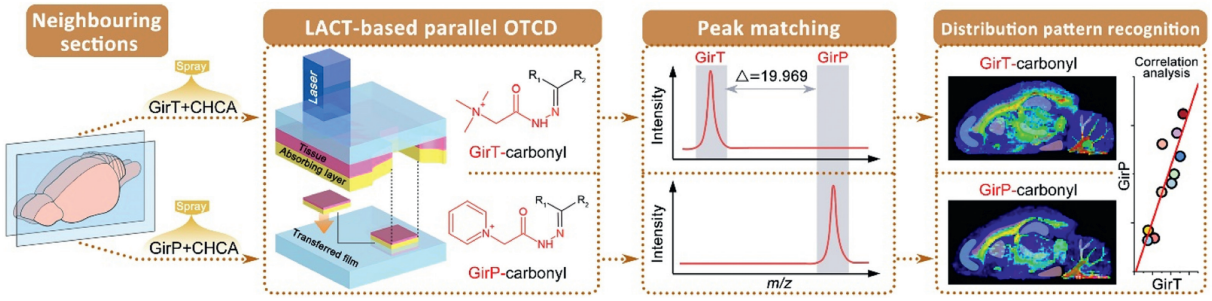

Fig. 1. Schematic workflow of LACT-based parallel OTCD of carbonyl metabolites for MALDI MSI. This workflow involves a four-step procedure: (1) The parallel derivatization reagents of GirT and GirP were deposited on the neighboring tissue sections, respectively; (2) LACT method was applied for the parallel OTCD; (3) a pair of candidate derivatized carbonyl metabolites was observed with the mass difference of 19.969 Da (±0.020 Da tolerance) in adjacent tissue sections; (4) the similarity of the distribution patterns between the GirT and GirP derivatives was calculated for further metabolite annotation.

the derivatized analytes to be transferred to a new acceptor slide [2,19]. This process enables an obvious sensitivity improvement and broader molecular coverage for MALDI MSI by removing the ionization competition/suppression from the endogenous tissue components and excess reagents (*e.g.*, MALDI matrix and derivatization reagent).

Moreover, incomplete reactions, excess derivatization reagents, as well as the complex tissue environment often lead to highly complex mass spectra and thus pose a greater challenge to metabolite identification and their spatial annotation [12]. *In situ* MS/MS analysis is widely used to address this challenge, however, it is limited by the quite low throughput and inadequate sensitivity to acquire meaningful fragment ions and their images [20,21]. Owing to the lack of purification and separation steps in liquid chromatography-mass spectrometry (LC-MS), conventional MSI methods are unavailable to distinguish interference compounds sharing the same *m/z* with derivatized metabolites, potentially resulting in ambiguous assignments of the spatial distribution of target ions in MSI [22,23]. Ion mobility spectrometry shows great promise in resolving isomeric compounds but this procedure requires an additional unconventional instrument and its resolution and sensitivity are limited in terms of small molecules [24]. Therefore, developing an annotation strategy for the OTCD MSI dataset with high efficiency and confidence is particularly important for understanding the submetabolome of biological tissues.

Parallel derivatization has become an ideal analytical strategy in LC-MS, owing to its capability to enhance the MS ionization efficiency and facilitate the accuracy and efficiency of molecular annotation [25]. In this work, a LACT-based parallel OTCD strategy was developed for MALDI MSI of the various derivatized carbonyl metabolites in brain tissue with high efficiency, high coverage, and confident spatial annotation. As illustrated in Fig. 1, a pair of derivatization reagents, Girard's T (GirT) and Girard's P (GirP), were used to parallelly derivatize carbonyls to obtain characteristic peak pairs with a regular mass difference of 19.969 Da, thus allowing the target screening of carbonyl derivatives utilizing mass-shift filtering. The similarity of the distribution pattern between parallelly derivatized metabolites was further statistically evaluated in neighboring tissue sections to narrow down the ambiguous metabolite annotations due to the occurrence of the interferences sharing the same nominal or exact mass, which guaranteed the reliability and accuracy of metabolite annotation.

A comparison of MALDI MS detection of carbonyl standards with and without GirT and GirP derivatization was first conducted to evaluate the LACT-based parallel OTCD strategy. The overall higher intensities of derivatized metabolites with a characteristic mass shift were obtained after derivatization compared to a non-derivatization method (Fig. S1 in Supporting information). To further reduce competitive ionization and ion suppression occurred in tissues, a LACT method developed by our group was applied to enhance OTCD performance and detection sensitivity of small molecules in MALDI MSI [2,19]. All animal experiments were carried out following the Guidelines for Animal Experimentation of China Pharmaceutical University (Nanjing, China) and approved by the Animal Ethics Committee of the Institution. As shown in Fig. 1, the mixture solutions of α-cyano-4-hydroxycinnamic acid (CHCA)/GirT and CHCA/GirP were separately sprayed on the neighboring brain sections by electro-assisted deposition. A focused laser (405 nm) was applied to illuminate the matrix-coated tissue placed on a donor slide in a transmission mode, and a thin film was transferred to another clean acceptor slide. LACT can effectively remove endogenous interferences from lipids and proteins in tissues and excessive derivatization reagent, and thus increase the detection sensitivity and molecular coverage. To comprehensively visualize the carbonyl metabolome in brain tissue, the LACT-based derivatization conditions were optimized, including the concentration of derivatization reagent, amount of matrix, and the laser power (Fig. S2 in Supporting information). Finally, the signal intensities of GirT and GirP derivatives reached a maximum at GirT (5 mg/mL)/CHCA (10 mg/mL) and GirP (5 mg/mL)/CHCA (10 mg/mL), and the continually increasing might cause severe suppression of the analyte signal. The laser output power ranging from 16 mW to 54 mW was tested, and 27 mW was sufficient to drive chemical transfer and derivatization. A comparison of the optimized LACT-based and the commonly used incubation-based OTCD was further performed. As shown in Fig. 2A, the dodecanal standard spotted on the brain cortex was used to compare detection sensitivity, and the signal intensities of GirT-dodecanal and GirP-dodecanal show a 2.44-fold and 6.90-fold increase by using LACT as compared with the incubation-based OTCD. Good linearity was achieved within the 100-fold concentration range ($R^2 > 0.99$) (Fig. 2B), indicating LACT-based OTCD could be used for the quantitation of carbonyl metabolites in tissues. Furthermore, a notable enhancement of molecular coverage (2.0-fold increase for GirT and 2.22-fold increase for GirP) resulted in a 3.31-fold increase in the number of ion pairs in comparison with incubation-based OTCD (Figs. 3A and B, Fig. S3 in Supporting information). Additionally, no analyte delocalization was observed when using LACT-based OTCD.

Fig. 3A shows the representative mass spectra obtained from the cerebral cortex region of rat brains after parallel OTCD with GirT and GirP, respectively. Multiple paired peaks with a 19.969 Da difference were assigned (labeled with the same color), and the candidate carbonyl-containing molecules could be readily recognized. As shown in Fig. 3B, 224 peaks of derivatized with GirT and 246 peaks of derivatized with GirP were observed in the cortex regions of neighboring brain sections. Mass-shift filtering was performed, and 119 ion pairs were obtained from the MALDI dataset, indicating that ~50% of detected features might be non-carbonyl

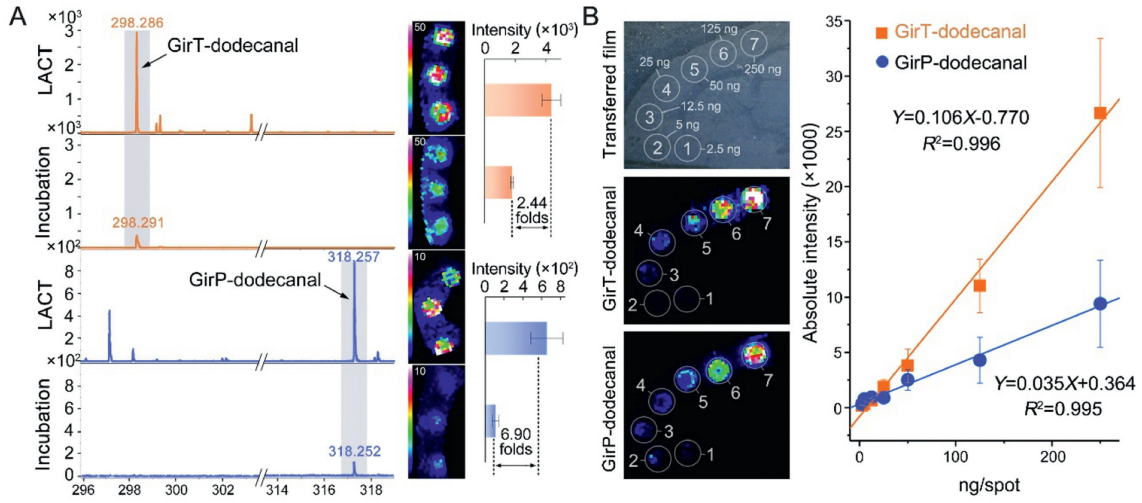

Fig. 2. (A) Comparison of average signal intensities of GirT-dodecanal and GirP-dodecanal obtained by using LACT-based and incubation-based OTCD. Error bars represent the standard deviation of average intensities of three replicate spots. (B) Quantitative calibration curves of GirT-dodecanal and GirP-dodecanal obtained by LACT in the range of 2.5–250 ng/spot. Error bars indicate the standard deviations of 20 mass spectra acquired from respective ions.

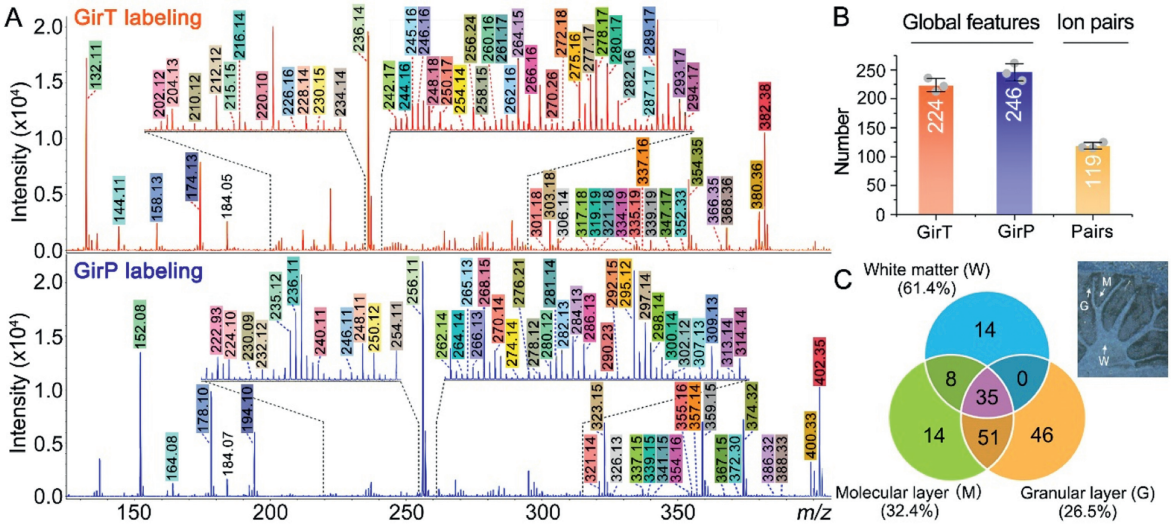

Fig. 3. (A) Representative mass spectra obtained from the cerebral cortex region of two neighboring brain tissue sections treated by LACT-based parallel OTCD. The detected ion pairs with 19.969 Da mass shift (±0.020 Da tolerance) labeled with the same color in correspondent mass spectra. (B) Number of the average detected features and ion pairs obtained by using the LACT-based parallel OTCD. The error bars indicate the standard deviations of three independent measurements. (C) Venn diagram illustrating the number of putatively identified carbonyl metabolites detected in white matter (W), granular layer (G), and molecular layer (M) of the cerebellum.

compounds. Therefore, LACT-based parallel OTCD provides an efficient method for the recognition of derivatized metabolites. Venn diagram revealed that only 35 common ion pairs occurred in white matter, granular layer, and molecular layer (three spatially adjacent areas in the cerebellum), accounting for 61.4%, 26.5%, and 32.4% of the total ion pairs in each region, indicating very high chemical heterogeneity in the cerebellum (Fig. 3C). These results demonstrated that LACT-based parallel OTCD provides a target and accurate approach to exploring spatial-chemical heterogeneity of carbonyl spatial submetabolome.

Although mass-shift filtering based on parallel OTCD is expected to remove the most of interference compounds, precise metabolite annotation is still hampered by the potential overlaps between derivatized analytes and interferents sharing the same nominal or exact mass. Therefore, the similarity in spatial distribution patterns of paired derivatized analytes can be used as the second criterion to improve the confidence of metabolite annotation. The proposed workflow for carbonyl metabolite annotation included 3 steps: STEP 1: Spatial segmentation of MSI data and extraction of *m/z* features from segmented subregions; STEP 2: screening paired derivatized analytes with the fixed mass shift; and STEP 3: metabolite annotation through the similarity comparison of spatial distribution patterns (Fig. 4).

Initially, two parallel MSI datasets (GirT and GirP) were subjected to spatial segmentation to classify and group all spectra by their similarity, and regions with distinct molecular compositions were coded with different colors. In Fig. 4A, almost identical segmentation results were obtained from GirT and GirP derivatization, and ten representative subregions were defined based on the MSI segmentation and anatomical structure (Fig. 4B). In STEP 1: The global *m/z* features of two parallel MSI datasets were extracted from each of the ten subregions, respectively, containing derivatized and interference compounds. Although the OTCD efficiency of GirT and GirP was somehow different, the comparable number of GirT- and GirP-derivatives were detected by MALDI MS in various subregions of rat brains (Figs. 3B and 4C). This result indicated that LACT-based OTCD could significantly enhance the detection sensitivity to compensate the derivatization differences be-

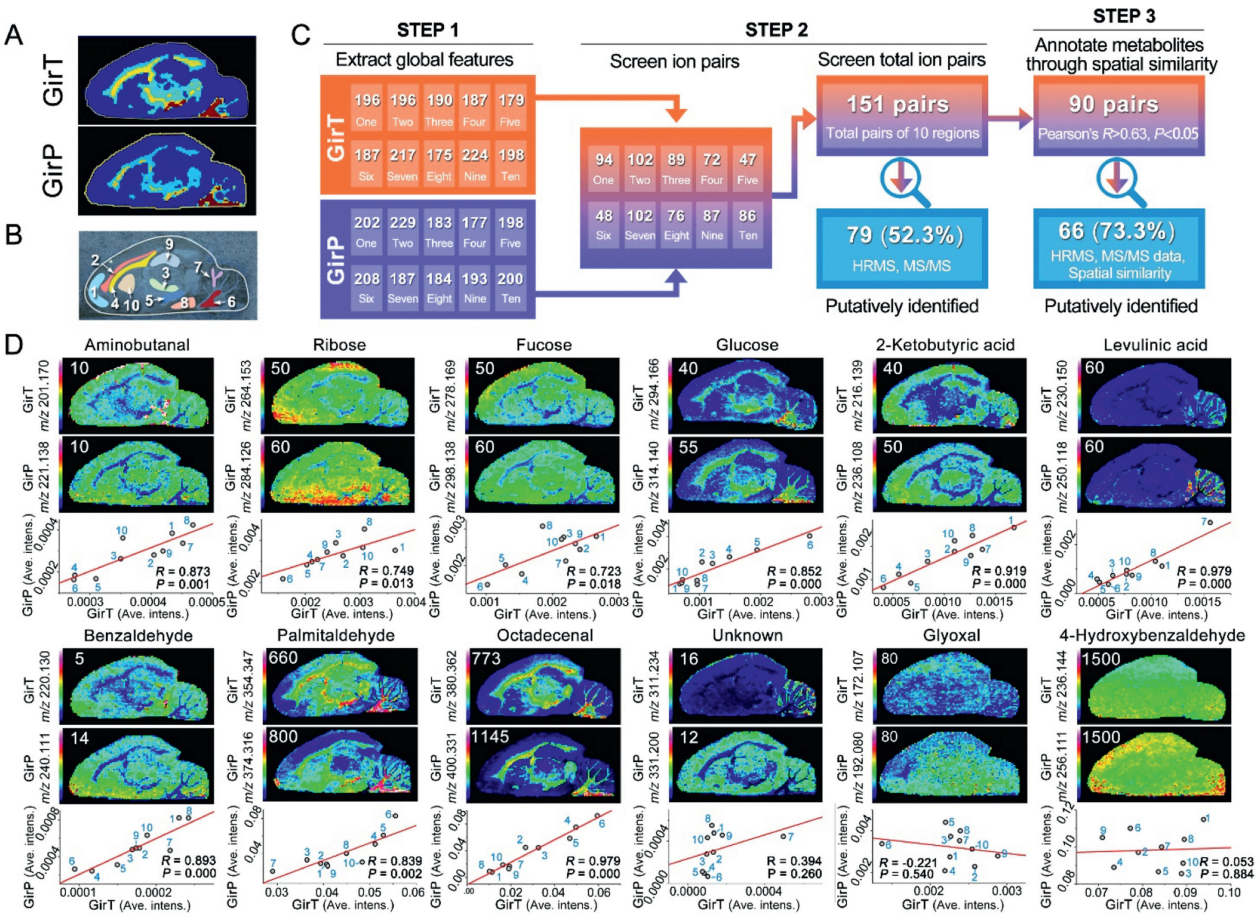

Fig. 4. Proposed workflow for carbonyl metabolite annotation. (A) Spatial segmentation of the neighboring brain sections after LACT-based parallel OTCD. (B) Assignment of representative subregions based on the segmentation result and anatomical structure. Ten subregions labeled as follows: 1, frontal cortex; 2, inner cortex; 3, thalamus; 4, corpus callosum; 5, hypothalamus; 6, cerebellum white matter; 7, cerebellum granular layer; 8, pons; 9, hippocampus; 10, caudate putamen. (C) STEP 1: Extraction of global *m/z* features from ten subregions; STEP 2: Screen of ion pairs based on the fixed mass shift; STEP 3: Calculation of similarity of spatial distribution patterns between the paired derivatives. (D) Representative ion images and spatial correlation analysis of the paired derivatives. The value of the color scale bar from the ion image represents the absolute intensity divided by 10.

tween GirT and GirP. The ideal solution to fully address the differences in derivatization efficiency is the application of isotope-labeled derivatization reagents but often paying a high cost for it. In STEP 2: 19.969 Da mass shift (±0.020 Da tolerance) was applied to rapidly screen candidate carbonyl metabolites. In this step, the number of paired derivatized analytes observed in the ten individual subregions ranged between 48 and 102, and over 50% of the interference compounds were removed by mass-shift filtering. In total, 151 paired derivatized analytes were obtained and putatively identified as carbonyl metabolites across ten subregions (Table S1 in Supporting information). Candidate carbonyl metabolites were putatively identified *via in situ* tandem MS of GirP derivatives using MALDI LIFT-TOF/TOF MS (Table S2 in Supporting information). GirP derivatives would yield a series of characteristic fragment ions including a common $[Py+H]^+$ ion at *m/z* 80, a neutral loss of 79 Da (Py), and GirP fragmentation patterns at *m/z* 120, *m/z* 137, and *m/z* 152 (Fig. S4 in Supporting information). MALDI FTICR MS was then used to acquire high-accuracy mass (<3 ppm) for *m/z* matching to the HMDB and MyCompoundID databases (Fig. S5 and Table S2 in Supporting information). Finally, 79 candidate carbonyl metabolites were putatively identified by accurate mass matching to metabolome databases and MS/MS spectra interpretation (Fig. 4C and Table S2).

In STEP 3: The similarity in spatial distribution patterns of paired derivatized analytes was determined by Pearson's correlation analysis. A Pearson's *R* greater than 0.63 with a *P*-value <0.05 indicates high spatial distribution similarity between the two compared images. The pairwise correlation of GirT and GirP peak intensities extracted from the ten subregions was calculated. Generally, the paired derivatized analytes with the 19.969 Da mass shift (±0.020 Da tolerance) and identical distribution showing a significant correlation ($R > 0.63$ and $P < 0.05$) could be readily and positively annotated as carbonyl metabolites. For instance, as shown in Fig. 4D, the spatial distribution patterns of GirT derivatives are similar to their correspondent GirP derivatives ($P < 0.019$), such as aminobutanal, ribose, fucose, 2-ketobutyric acid, and benzaldehyde, which are mainly accumulated in the cerebral cortex, pons and hippocampus. Likewise, GirT and GirP derivatives of glucose, palmitaldehyde, and octadecenal exhibited highly similar distribution patterns ($P < 0.003$), which are confined in the corpus callosum and hypothalamus. On the other hand, the ion pairs satisfied the mass shift of 19.969 Da but showed different distribution patterns, such as unknown paired analytes (*m/z* 311.234 and *m/z* 331.200) ($P = 0.260$) (Fig. 4D). Besides, although some ion pairs were putatively identified as carbonyl metabolites based on the accurate mass matching and characteristic fragmentation patterns, their distribution patterns were still different (*e.g.,* glyoxal, $P = 0.540$ and 4-hydroxybenzaldehyde, $P = 0.884$), indicating that individual ion image may contain overlapped interferences, such as a matrix peak of *m/z* 172.04, that would distort the true spatial

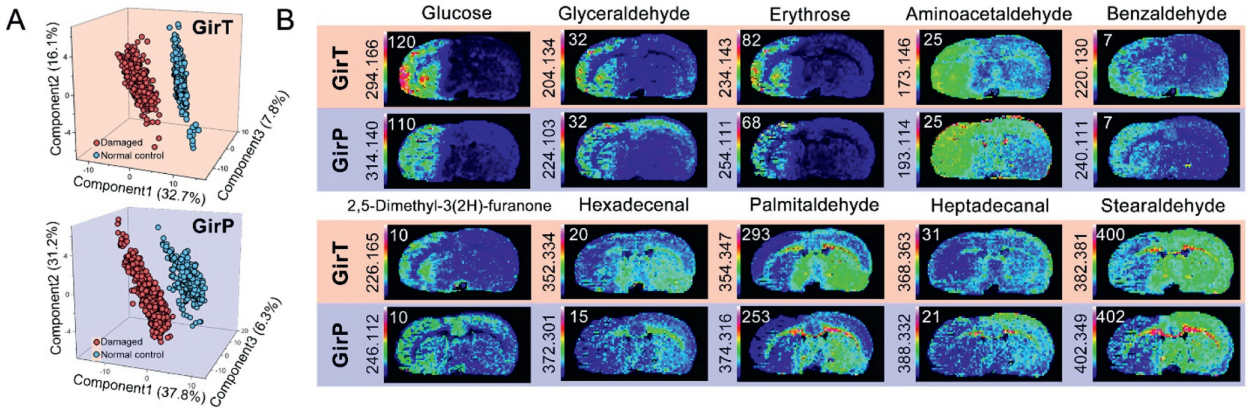

Fig. 5. MALDI MSI of selected carbonyl metabolites in coronal brain section of middle cerebral artery occlusion (MCAO) rat treated with GirT and GirP, respectively. (A) Partial least squares discriminant analysis (PLS-DA) models to discriminate GirT and GirP derivatized carbonyl metabolites in the damaged region (red dots) and adjacent normal control (blue dots), respectively. (B) Paired ion images of ischemic-associated carbonyl metabolites with VIP score of PLS-DA > 1.

distribution pattern of target metabolites (Fig. 4D) [26]. Finally, a total of 90 ion pairs were found to possess identical distribution patterns, while 61 ion pairs ($P > 0.05$) were excluded from the 151 ion pairs (Table S1). Among 90 candidate carbonyl metabolites, 66 (73.3%) were putatively identified by MS/MS analysis and database searching based on accurate mass matching (<3 ppm) (Table S2), including aldehydes, ketones, dicarbonyls, oxo acids, saccharides, and other specific carbonyls (*e.g.*, furanone). Most of the identified carbonyl metabolites (43 out of 66) have been reported previously in human and animal species, but their spatial distributions were first observed in the rat brain tissue (Tables S1 and S2). For example, monosaccharides, possessing a variety of biological activity and functional characteristics, showed diverse distribution patterns. As shown in Fig. 4D, fucose and ribose distributed across the cerebral cortex, pons, hippocampus, and caudate putamen, whereas glucose exhibited an opposite pattern with high abundance in the corpus callosum, thalamus, and cerebellum white matter, which was in agreement with previous studies [27,28]. 2-Ketobutyric acid was mainly located in the cerebral cortex, caudate putamen, and hippocampus, whereas levulinic acid was found to be specially located in the granular layer of the cerebellum. Besides, benzaldehyde and aminobutanal were notably enriched in the cerebral and cerebellar cortex, whereas long-chain fatty aldehydes such as palmitaldehyde and octadecenal were abundant in the inner cortex, corpus callosum, thalamus, and cerebellum white matter. In terms of the remaining 24 unidentified candidate carbonyl metabolites, their molecular identity was not found in the databases, indicating they might be the potential unreported carbonyls, and further investigation is required (Table S2).

Stroke has become a critical public health issue leading to disability and death [29]. Significant metabolic disturbances occurred in brain ischemia, such as abnormal changes in levels of aldehydes and ketones particularly in injured areas [30,31]. Herein, to broaden its applicability, the developed LACT-based parallel OTCD method was applied to a rat model of ischemia/reperfusion (IR) injury for a comprehensive investigation of the spatio-chemical perturbation of carbonyl metabolites, which is rarely investigated. As shown in Fig. 5A and Fig. S6A (Supporting information), the damaged and adjacent normal regions were unambiguously segregated into two tight clusters in both GirT and GirP-treated tissue samples, confirming that endogenous carbonyl metabolites were changed after IR injury. The metabolites with a variable importance in the projection (VIP) score higher than 1, higher fold change (FC) value, and the same alteration trend between GirT and GirP groups in Y-scatterplots were identified as differential metabolites (Fig. S6B in Supporting information) [32]. As expected, the changed carbonyl metabolites showed almost identical spatial distribution patterns between GirT and GirP derivatives in the damaged region, indicating the applicability of LACT-based parallel OTCD for identifying metabolite signatures associated with brain disease (Fig. 5B). Glucose was found to be the most discriminant variable exhibiting elevated level in the damaged region, which is consistent with the previous findings [27,28]. Other monosaccharides such as erythrose and glyceraldehyde showed a similar spatial change in rat brain subjected to IR injury, indicating that occlusion of the middle cerebral artery may result in the destruction of the aerobic oxidation process and eventually lead to the decreased utilization and subsequent abnormal accumulation of monosaccharides in the IR region [28,33]. Volatile and small molecule aldehydes/ketones usually contribute to the progress of oxidative stress-associated diseases but are inaccessible in common metabolomics analyses [34,35]. The developed method revealed the spatial changes of aminoacetaldehyde, benzaldehyde, and 2,5-dimethyl-3(2*H*)-furanone, and they show abnormal accumulation in the damaged region. These over-produced molecules are associated with increased oxidative damage in stroke [36]. Lipid metabolism is of particular importance for the central nervous system, and fatty aldehydes are important precursors for lipid synthesis. MALDI MSI results showed that long-chain fatty aldehydes containing 16–18 carbons decreased in the ischemic hemisphere, especially in the cerebral cortex. This result was consistent with previous findings about decreased levels of long-chain lipids such as phosphatidylethanolamine (PE) (18:0/22:6) and phosphatidylserine (PS) (18:0/22:6) in the ischemic brain [37]. Therefore, LACT-based parallel OTCD provides an advantageous combination of sensitivity and accuracy for MALDI MSI and subsequent annotation of target spatial submetabolome, which should help investigate molecular mechanisms in neurological diseases.

In conclusion, we developed a LACT-based parallel OTCD strategy for profiling and mapping the carbonyl submetabolome in biological tissues with high sensitivity and molecular coverage, as well as facilitating the metabolite annotation with high efficiency and accuracy. This strategy is based on parallel derivatization by using GirT and GirP, resulting in the generation of a pair of derivatives with a 19.969 Da interval for the accurate and rapid identification of candidate carbonyl metabolites in tissue samples. Due to the pretreatment with LACT, the suppression effects derived from complex tissue components and excessive chemical reagents could be effectively reduced, and consequently, 151 ion pairs in selected subregions of rat brains were localized. The similarity of spatial distribution patterns between GirT and GirP derivatives was further calculated to remove interference compounds. A total of 90

carbonyl metabolites were finally identified and visualized in rat brain tissue with high reliability. Moreover, the spatial perturbations of these rarely detected carbonyls in ischemic regions in a rat model of stroke were revealed. All these results indicate that parallel OTCD enables an efficient and accurate characterization and mapping of the submetabolome of biological tissue.

Declaration of competing interest

The authors declare that they have no known competing financial interests or personal relationships that could have appeared to influence the work reported in this paper.

Acknowledgment

This work was supported by the National Natural Science Foundation of China (Nos. 82374028 and 81803957).

Supplementary materials

Supplementary material associated with this article can be found, in the online version, at doi:10.1016/j.cclet.2024.110366.

References

[1] W.H. Müller, A. Verdin, E. De Pauw, et al., Mass Spectrom. Rev. 41 (2022) 373–420.
[2] S. Guo, K. Li, Y. Chen, et al., Acta. Pharm. Sin. B 12 (2022) 2120–2126.
[3] B. Li, E.K. Neumann, J. Ge, et al., Plant Cell Environ. 41 (2018) 2693–2703.
[4] W. Tang, J.J. Shi, W. Liu, et al., Angew. Chem. Int. Ed. 62 (2023) e202301309.
[5] A.J. Taylor, A. Dexter, J. Bunch, Anal. Chem. 90 (2018) 5637–5645.
[6] X. Wang, J. Han, J. Yang, et al., Chem. Sci. 6 (2015) 729–738.
[7] J. He, C. Sun, T. Li, et al., Adv. Sci. 5 (2018) 1800250.
[8] Y. Chen, W. Tang, A. Gordon, et al., J. Am. Soc. Mass Spectrom. 31 (2020) 1066–1073.
[9] R. Sun, W. Tang, P. Li, et al., Anal. Chem. 95 (2023) 16004–16012.
[10] J. Soltwisch, H. Kettling, S. Vens-Cappell, et al., Science 348 (2015) 211–215.
[11] Y. Wang, S. Li, K. Qian, Nanoscale Adv. 5 (2023) 6804–6818.
[12] C. Harkin, K.W. Smith, F.L. Cruickshank, et al., Mass Spectrom. Rev. 41 (2022) 662–694.
[13] G. Ma, X. Zhao, M. Guo, et al., Anal. Chim. Acta 1201 (2022) 339620.
[14] J. Huang, S. Gao, K. Wang, et al., Chin. Chem. Lett. 34 (2023) 107865.
[15] J. Liu, Q. Zang, X. Li, et al., Chin. Chem. Lett. 34 (2023) 108322.
[16] Q. Zang, M. Wang, Y. Zhu, et al., Anal. Chem. 93 (2021) 15373–15380.
[17] Y.Q. Cao, Y.J. Lu, L. Zhang, et al., Chin. Chem. Lett. 35 (2024) 109788.
[18] Q. Wu, T.J. Comi, B. Li, et al., Anal. Chem. 88 (2016) 5988–5995.
[19] K. Li, S. Guo, W. Tang, et al., Chem. Commun. 57 (2021) 12460–12463.
[20] B. Li, J. Ge, W. Liu, et al., New Phytol. 231 (2021) 892–902.
[21] B. Li, D.R. Bhandari, C. Janfelt, et al., Plant J. 80 (2014) 161–171.
[22] B.S.R. Claes, E. Takeo, E. Fukusaki, et al., Mass Spectrom. 8 (2019) A0078.
[23] L. Feldberg, Y. Dong, U. Heinig, et al., Anal. Chem. 90 (2018) 10231–10238.
[24] D.Mesa Sanchez, S. Creger, V. Singla, et al., J. Am. Soc. Mass Spectrom. 31 (2020) 2437–2442.
[25] M.F.C. Girard, D. Ruskic, G. Böhm, et al., Anal. Chim. Acta 1127 (2020) 198–206.
[26] Z. Guo, Q. Zhang, H. Zou, et al., Anal. Chem. 74 (2002) 1637–1641.
[27] L. Wang, T. Zhu, H.B. Xu, et al., Ann. Transl. Med. 9 (2021) 246.
[28] F. Tian, R. Liu, C. Fan, et al., Metabolites 10 (2020) 27.
[29] T.M. Woodruff, J. Thundyil, S.C. Tang, et al., Mol. Neurodegener. 6 (2011) 11.
[30] K. Uchida, Free Radic, Biol. Med. 28 (2000) 1685–1696.
[31] E. Baranovicova, D. Kalenska, P. Kaplan, et al., Int. J. Mol. Sci. 24 (2023) 17302.
[32] S. Guo, Y. Wang, D. Zhou, et al., Sci. Rep. 4 (2014) 5959.
[33] T. Zhu, L. Wang, F. Tian, et al., Biomed. Pharmacother. 129 (2020) 110470.
[34] W. Lin, L.P. Conway, A. Block, et al., Analyst 145 (2020) 3822–3831.
[35] W. Lin, L.P. Conway, M. Vujasinovic, et al., Angew. Chem. 133 (2021) 23420–23428.
[36] A. Cherubini, C. Ruggiero, M.C. Polidori, et al., Free Radic. Biol. Med. 39 (2005) 841–852.
[37] S. Guo, D. Zhou, M. Zhang, et al., Sci. Rep. 7 (2017) 5054.